Electronic band structure of a Tl/Sn atomic sandwich on Si(111)

D. V. Gruznev,[1,2] L. V. Bondarenko,[1,2] A. V. Matetskiy,[1,2] A. Y. Tupchaya,[1,2] A. A. Alekseev,[1] C. R. Hsing,[3] C. M. Wei,[3]
S. V. Eremeev,[4,5] A. V. Zotov,[1,2,6] and A. A. Saranin[1,2]

[1]*Institute of Automation and Control Processes FEB RAS, 690041 Vladivostok, Russia*
[2]*School of Natural Sciences, Far Eastern Federal University, 690000 Vladivostok, Russia*
[3]*Institute of Atomic and Molecular Sciences, Academia Sinica, P.O. Box 23-166 Taipei, Taiwan*
[4]*Institute of Strength Physics and Material Science, 634021 Tomsk, Russia*
[5]*Tomsk State University, 634050 Tomsk, Russia*
[6]*Department of Electronics, Vladivostok State University of Economics and Service, 690600 Vladivostok, Russia*

A two-dimensional compound made of one monolayer of Tl and one monolayer of Sn on Si(111) has been found to have a sandwichlike structure in which the Sn layer (having the milk-stool arrangement) resides on the bulklike terminated Si(111) surface and the Tl layer (having the honeycomb-chained-trimer arrangement) is located above the Sn layer. The electronic band structure of the compound contains two spin-split surface-state bands, of which one is nonmetallic and the other is metallic. Near the Fermi level the metallic band is split with the momentum splitting $\Delta k_\parallel = 0.037$ Å^{-1} and energy splitting $\Delta E_{\rm F} = 167$ meV. The steep dispersion of the band when crossing the Fermi level corresponds to an electron velocity of $\approx 8.5 \times 10^5$ m/s, which is comparable to the value reported for graphene. The 2D Fermi contours have almost circular shape with spin texture typical for hexagonal surfaces.

I. INTRODUCTION

Discovery of graphene has stimulated the enhanced interest to other possible atomically thin, two-dimensional (2D) materials. 2D monolayer structures of metals on semiconductor (e.g., silicon and germanium) surfaces provide vivid examples. A set of fascinating phenomena has recently been found in these material systems as follows. At the one monolayer (1 ML) In/Si(111) surface, the metal-insulator (4×1 to "8×2") transition has been found [1,2] in which the physical mechanism remains a debated subject till now [3,4]. The $\sqrt{3} \times \sqrt{3}$ to 3×3 transition taking place in the 1/3-ML Pb/Si(111) system has also attracted substantial interest [5,6]. Dynamics of a dense 2D Pb layer on Si(111) has been found to obey an exceptional collective superdiffusive mechanism [7–10]. In the same Pb layer realization of nearly massless electrons has been demonstrated [11] and 2D superconductivity has been observed [as well as in the 2D In/Si(111) system] [12–15]. A large Rashba-type spin splitting of surface-state bands has been detected at the Bi/Si(111) [16,17], Tl/Si(111) [18,19], Pt/Si(110) [20], Pb/Ge(111) [21], and Au/Ge(111) [22] surfaces, giving promise for their potential application in the silicon-based spintronics devices. Natural expansion of the research field associated with 2D metal layers on semiconductors resides in addressing multimetal systems. Adding appropriate species to a given metal layer might change its properties in a desired way. For example, it has been demonstrated that originally poor structural and electronic properties of an Au/Si(111)$\sqrt{3} \times \sqrt{3}$ surface are substantially improved by adsorbing small amounts of Tl, In, Na, or Cs [23]. Even more promising possibilities can be expected for ordered 2D alloys. Being fully characterized [e.g., as in the case of Sn-Ag alloy on Si(111)] the 2D compounds represent a class of low-dimensional materials with advanced properties [24]. For example, an electron velocity at the Fermi level for the Sn-Ag 2D alloy [24] is comparable to the value reported for graphene.

Very recent theoretical studies on hypothetical Bi-(Cl, Br, I)/Si(111) [25] and Bi-H/Si(111) [26] systems predict that 2D compounds on Si(111) might demonstrate very exotic properties, e.g., show up as large-gap quantum spin Hall insulators. The Bi-Na and Tl-Pb 2D compounds on Si(111) have been found to possess spin-split *metallic* surface-state bands [27], in contrast to the most single-metal 2D layers on Si(111) (e.g., Bi/Si(111) [16,17], Tl/Si(111) [18,19], Pt/Si(110) [20]) in which only the *nonmetallic* bands are spin-split.

In this paper we are presenting a fully characterized specific 2D Tl-Sn compound which has a sandwichlike structure where Tl monolayer resides atop a Sn monolayer located above a bulk-truncated Si(111) surface. Within the bottom layer, Sn atoms occupy basic on-top (T_1) sites to form trimers centered in H_3 sites (forming a so-called milk-stool structure). Tl atoms in the top layer sit above T_4 sites and are arranged into the honeycomb-chained-trimer structure with Tl trimers centered in H_3 sites. The main features of the 2D compound electronic band structure are the two spin-split surface-state bands, of which the one is nonmetallic and the other is metallic. Near the Fermi level the latter band is split with the momentum splitting $\Delta k_\parallel = 0.037$ Å^{-1} and energy splitting $\Delta E_{\rm F} = 167$ meV. The steep dispersion of the band when crossing the Fermi level corresponds to an electron velocity of $\approx 8.5 \times 10^5$ m/s, which is comparable to the value reported for graphene.

II. EXPERIMENTAL AND CALCULATION DETAILS

The scanning tunneling microscopy (STM), low energy electron diffraction (LEED), and angle-resolved photoelectron spectroscopy (ARPES) experiments were performed in an ultrahigh-vacuum Omicron MULTIPROBE system with a base pressure better than $\sim 2.0 \times 10^{-10}$ Torr. Atomically clean Si(111)7×7 surfaces were prepared *in situ* by flashing to 1280 °C after the samples were first outgassed at 600 °C
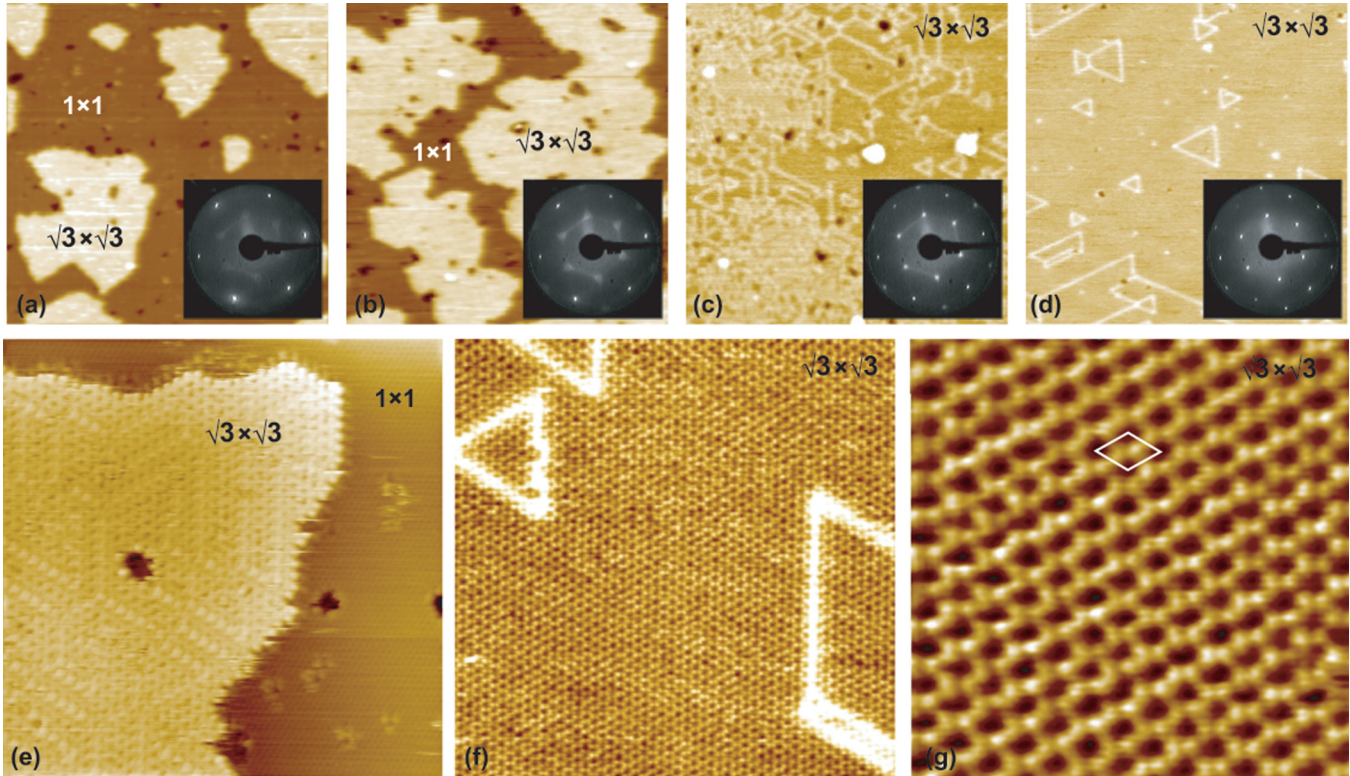
FIG. 1. (Color online) Formation of the Tl-Sn 2D compound on Si(111). 100×100 nm^2 STM images showing the Tl/Si(111)1×1 surface after depositing (a) 0.2 ML, (b) 0.5 ML, (c) 0.8 ML, and (d) 1.0 ML Sn. Insets show LEED patterns ($E_p = 41$ eV) from the corresponding surfaces. Regions of 1×1-Tl and $\sqrt{3} \times \sqrt{3}$-(Tl, Sn) are indicated. High-resolution 25×25 nm^2 STM images showing the structure of the surface after depositing (e) 0.5 ML and (f) 1.0 ML Sn. (g) 8×8 nm^2 STM image of the final Tl-Sn compound.

for several hours. Pristine Tl/Si(111)1×1 reconstruction was formed by depositing 1 ML Tl from a tantalum tube onto the Si(111)7×7 surface held at $\sim 300\,°$C. [1 ML (monolayer) $= 7.8 \times 10^{14}$ cm^{-2}.] Tin was deposited from a Mo boat. Sn deposition rate (with accuracy of $\sim 15\%$) was calibrated using STM observations of the $\sqrt{3} \times \sqrt{3}$-Sn phase formation on Si(111). STM images were acquired using Omicron variable-temperature STM-XA operating in a constant-current mode. Electrochemically etched W tips and mechanically cut PtIr tips were used as STM probes after annealing in vacuum. ARPES measurements were conducted using a VG Scienta R3000 electron analyzer and high-flux He discharge lamp ($h\nu = 21.2$ eV) with a toroidal-grating monochromator as a light source.

Density functional theory calculations with spin-orbit coupling effect were performed using projector-augmented-wave (PAW) [28,29] potentials, as implemented in the Vienna *ab initio* simulation package (VASP) [30,31]. The scalar relativistic effect was incorporated into the PAW potentials. In order to find the most stable structures of each (Tl, Sn)/Si(111) configuration with different Tl and Sn coverages, we used the *ab initio* random structure searching (AIRSS) [32] method which has already proven to be an efficient and effective method for exploring unanticipated structures of solids [33], point defects [34], surfaces [35,36], and clusters [37]. The (Tl, Sn)/Si(111)$\sqrt{3} \times \sqrt{3}$ supercell geometry was simulated by a repeating slab of five Si bilayers and a vacuum region of ~ 15 Å. Si atoms in the bottom two bilayers were fixed at their

bulk positions, top three bilayers were allowed to fully relax, and dangling bonds on the bottom surface were saturated by hydrogen atoms. The kinetic cutoff energy was 400 eV, and a Monkhorst-Pack $6 \times 6 \times 1$ k-point mesh was used to sample the surface Brillouin zone within AIRSS. The geometry optimization is performed until the residual force was smaller than 10 meV/Å. For band structure calculation on the stable (Tl, Sn)/Si(111) structure the k mesh and substrate thickness were increased up to $9 \times 9 \times 1$ and six Si bilayers, respectively.

III. RESULTS AND DISCUSSION

Deposition of 1 ML Sn onto the Tl/Si(111)1×1 surface leads to formation of the 2D Tl-Sn compound with $\sqrt{3} \times \sqrt{3}$ structure periodicity. The compound formation takes place already at room temperature, however $150\,°$C is more appropriate for improving structural properties of the compound. When there is a deficiency of Sn, the local patches of the compound form [Fig. 1(a)], which grow in size with Sn deposition. At $\sim 2/3$ ML Sn, the entire surface becomes occupied by the Tl-Sn compound. At that moment, the compound layer contains a high density of the domain walls seen in STM images as light meandering lines. The LEED pattern from this surface displays $\sqrt{3}$ spots connected by streaky features. Note that the domain walls are present already in the patches of the Tl-Sn compound growing at the early stages of Sn deposition. Upon further Sn deposition, the density of domain walls decreases and at ~ 1.0 ML Sn the
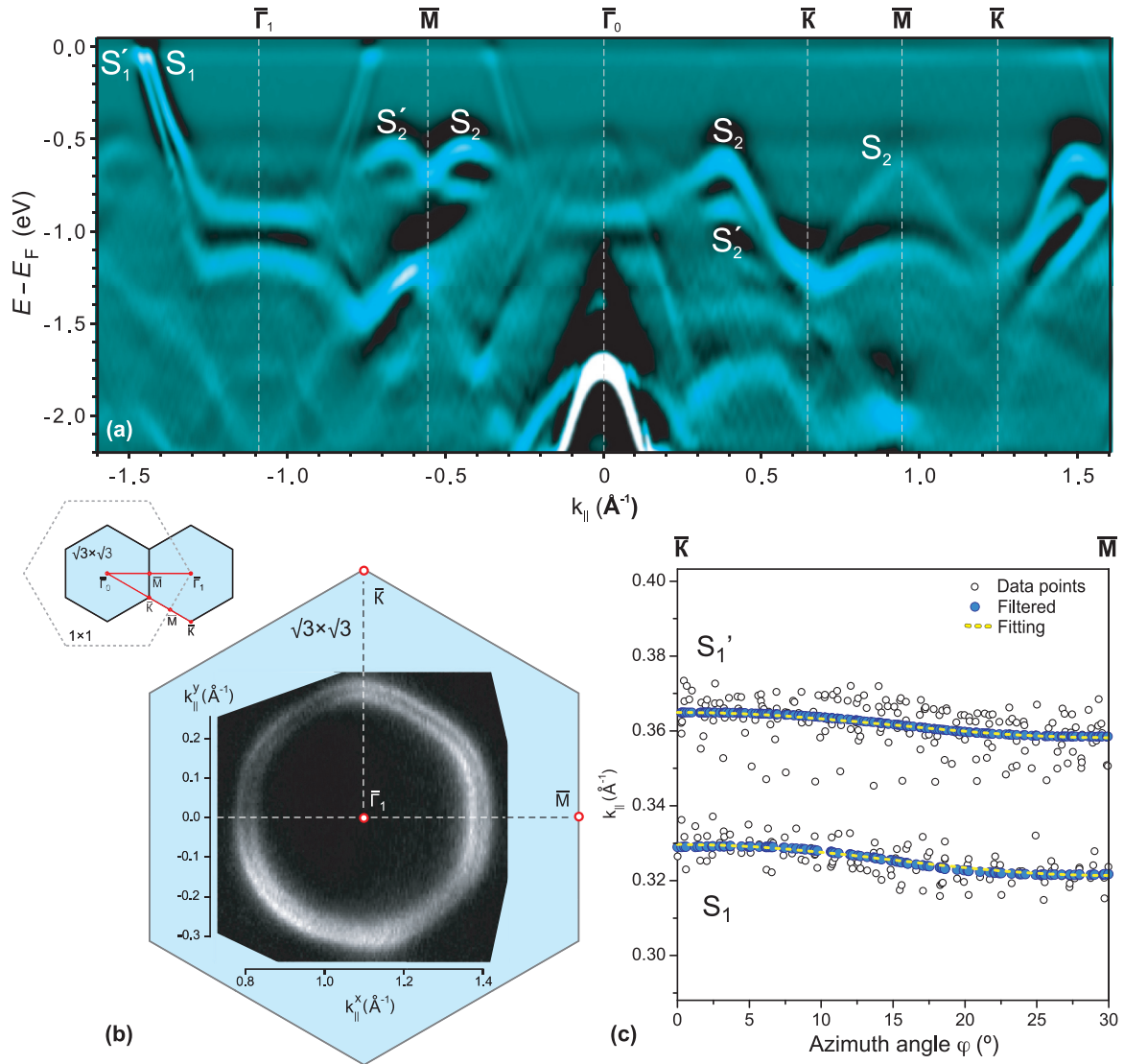
FIG. 2. (Color online) Experimental ARPES results on the electronic band structure of the Tl-Sn 2D compound on Si(111). (a) Second derivative of the photoemission intensity map taken along the directions indicated by red lines in the sketch of reciprocal space geometry with boundaries of the $\sqrt{3} \times \sqrt{3}$ and 1×1 SBZs given by solid black and dashed blue lines, respectively. (b) Fermi contour obtained with ARPES. (c) Azimuthal dependence of the Fermi wave vector length ($k_{\parallel}$). Open circles show experimental raw values, blue circles are obtained by FFT filtering the experimental values, and dotted yellow lines fit the experimental data according to the $k + \Delta k \cos(6\phi)$ expression with $k = 0.3616$ Å^{-1} and $\Delta k = 0.0034$ Å^{-1} for the S_1 band and $k = 0.3247$ Å^{-1} and $\Delta k = 0.0033$ Å^{-1} for the S_1' band.

homogeneous surface almost free of domain walls develops. It displays a LEED pattern with sharp spots and no other features. As for the high-resolution STM observations, we were able to acquire STM images only at low bias voltages of less than ~ 0.1 V. The Tl-Sn compound surface displays basically a honeycomblike structure in both polarities. It is worth noting, however, that an STM appearance of the surface often changes during scanning which means that the tip effects might play a noticeable role during STM image acquisition.

ARPES observations revealed that all spectral features become sharp and distinct only when formation of the Tl-Sn compound is completed (i.e., at 1.0 ML Sn). The two split surface-state bands in the Si bulk gap S_1 (S_1') and S_2 (S_2') constitute the main features of the (Tl, Sn)/Si(111) electronic band structure. The latter band S_2 (S_2') is nonmetallic. This

band resided at the $\bar{M}$ and $\bar{K}$ points at ~ -0.70 and ~ -1.25 eV, respectively, splits into two components when moving away from the high-symmetry points, which is thought to be a strong indication of the Rashba-type splitting. By characterizing the band split using Rashba energy E_R and the momentum offset k_0, one obtains for S_2 (S_2') band $E_R = 83$ meV and $k_0 = 0.096$ Å^{-1}. Remarkably, the shape and even the splitting values of this S_2 (S_2') band are similar to those of the surface-state band of the chemically very different system, namely, the β-Bi/Si(111)$\sqrt{3} \times \sqrt{3}$ reconstruction [16,17].

The other band S_1 (S_1') is metallic. It is centered around the $\bar{\Gamma}$ point and crosses the Fermi level at $k_F \sim 0.32$ (0.36) Å^{-1}. The steep dispersion of the band when crossing the Fermi level corresponds to an electron velocity of $\approx 8.5 \times 10^5$ m/s which exceeds slightly the value $\approx 7.8 \times 10^5$ m/s reported for the
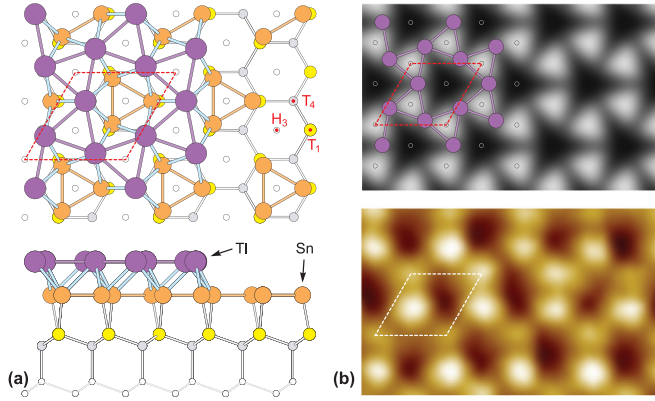
FIG. 3. (Color online) Atomic structure of the Tl-Sn 2D compound on Si(111). (a) Top and side views of the structural model of the Tl-Sn compound built of 1.0 ML Tl and 1.0 ML Sn. Tl atoms are shown by violet circles, Sn atoms by orange circles, top Si atoms by yellow circles, and deeper Si atoms by small gray and white circles. The $\sqrt{3} \times \sqrt{3}$ unit cell is outlined by a red frame. (b) Comparison of the simulated (upper panel) and experimental (lower panel) STM images. In the upper panel the model is superposed with the simulated image.

Sn-Ag alloy on Si(111) [24] and is comparable to the value $\approx 1 \times 10^6$ m/s reported for graphene. Near the Fermi level, the band is split with the momentum splitting $\Delta k_\parallel = 0.037$ Å^{-1} and energy splitting $\Delta E_F = 167$ meV. Figure 2(b) shows the ARPES Fermi surface of the compound which contains two concentric contours corresponding to S_1 and S_1' bands. At a glance, both contours look as circular loops, but actually
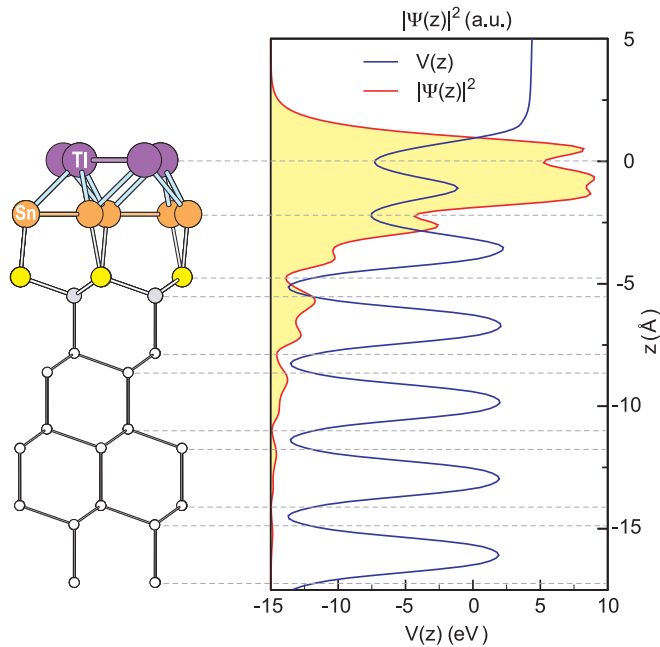

FIG. 4. (Color online) In-depth distribution of the electron density $|\Psi(z)|^2$ (red line) and potential $V(z)$ (blue line) in relation to the atomic structure of the Tl-Sn 2D compound located on the four Si bilayers. Tl atoms are shown by violet circles, Sn atoms by orange circles, top Si atoms by yellow circles, and deeper Si atoms by small gray and white circles.

TABLE I. (Color online) Structural models, symmetries, and formation energies of the nonstochiometric Tl-Sn 2D compounds on Si(111), as revealed by AIRSS method. Compound compositions are given by numbers of atoms in the $\sqrt{3} \times \sqrt{3}$ unit cell. Sequence of the structures in the table follows the decrease in the formation energies. Colors of the circles showing Tl, Sn, and Si atoms are the same as in Fig. 3.

Tl	Sn	Model	Sym.	E_f, eV
3	1		C_{3v}	-1.950
2	2		C_{1h}	-1.956
3	2		C_{1h}	-2.036
1	3		C_{3v}	-2.199
2	3		C_{3v}	-2.338
3	3	see Fig. 3(a)	C_{3v}	-2.549

they are smoothed hexagons which are typical for the known examples of the spin-split metallic bands on silicon and germanium. Thus, the contour shape can be described as $k + \Delta k \cos(6\phi)$. However, deviation from the circle is very small, $\Delta k / k \sim 1.0\%$.

In order to elucidate an atomic structure of the (Tl, Sn)/Si(111) surface, we applied the AIRSS technique using the knowledge on the compound compositions. Consider first
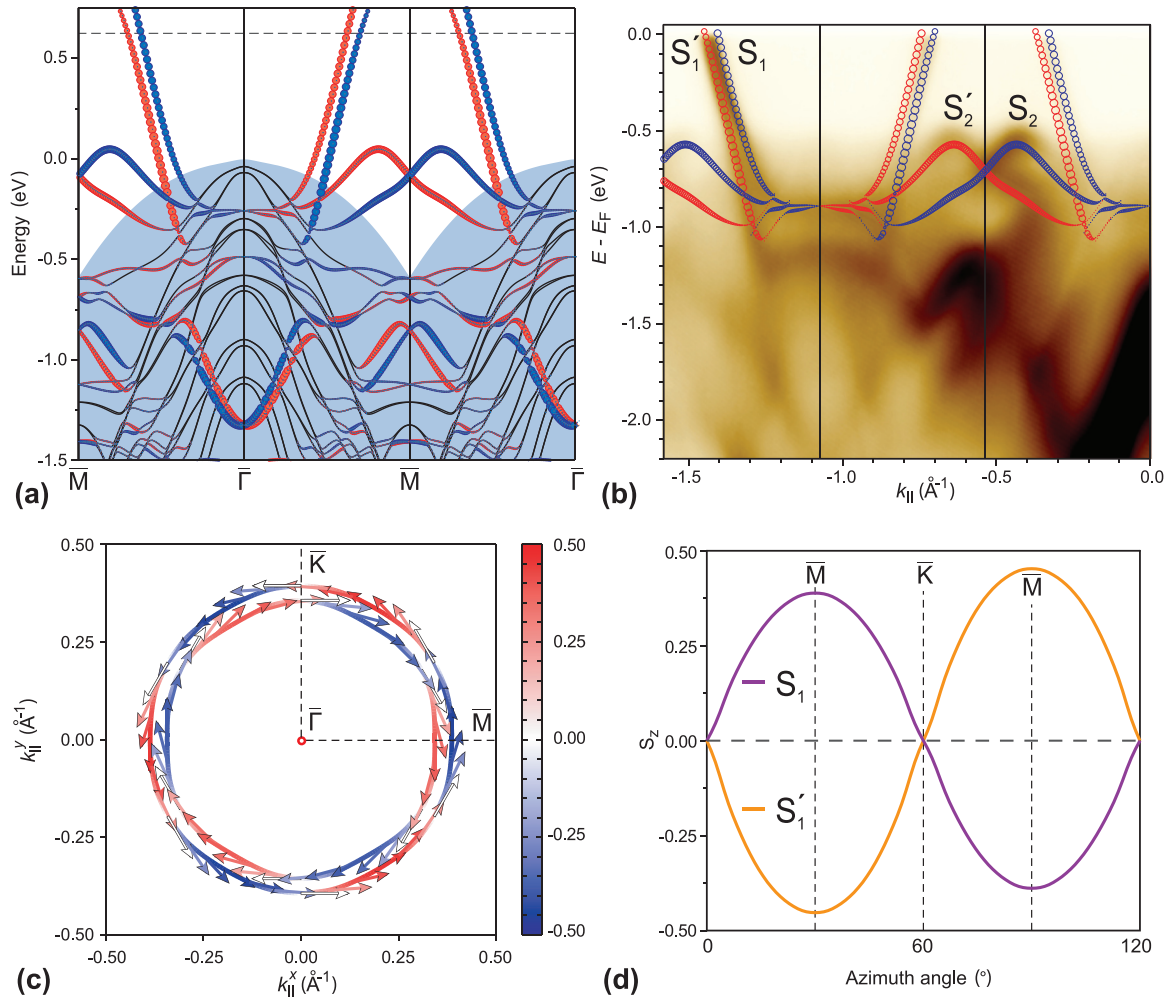
FIG. 5. (Color online) Results of the DFT calculations. (a) Calculated band structure of the Tl-Sn 2D compound on Si(111). The bands with opposite spin orientation are highlighted by blue and red circles. The size of the circles corresponds to the strength of the surface character summed over all orbitals at a particular $k_\parallel$ value. Shaded region indicates projected bulk bands. (b) Calculated dispersions of S_1 and S_2 bands superposed with the corresponding ARPES spectrum. (c) Calculated Fermi contour. Arrows adjacent to the contour and their length denote the in-plane spin component. The out-of-plane spin component is indicated by the color with red and blue corresponding to the upward and downward directions, respectively. White color indicates fully in-plane alignment. (d) Azimuthal dependencies of the out-of-plane spin component for the S_1 and S_1' bands.

the final structure, containing 1 ML Tl and 1 ML Sn (i.e., three Tl atoms and three Sn atoms per $\sqrt{3} \times \sqrt{3}$ unit cell). The most stable configuration found for this surface is shown in Fig. 3(a). One can see that this is essentially a sandwichlike double-layer structure containing Sn (bottom) and Tl (top) layers on a Si(111) surface. The Sn layer resides 2.55 Å above the top Si atoms and Tl atoms are 2.21 Å higher than Sn atoms. Residence of the Sn layer below the Tl layer implies that when adsorbing onto the Tl/Si(111)1 × 1 surface Sn atoms penetrate through the Tl layer and substitute Tl atoms in the metal-silicon bonds. Within the bottom layer Sn atoms occupy basic on-top (T_1) sites to form trimers having a side length of 2.99 Å and centered in the H_3 sites. Tl atoms in the top layer sit above Si(111) T_4 sites and are arranged into the honeycomb-chained-trimer structure where Tl trimers are centered also in the H_3 sites. The side length of the Tl trimer is 3.49 Å and the trimers are twisted in the surface plane by $\pm 10.9°$. Simulated STM image of the model demonstrates

a honeycomblike appearance of the surface [Fig. 3(b)] in agreement with the experimental STM data. A structure similar to this model but with the Tl and Sn trimers centered in the T_4 sites constitutes the next low-energy configuration with its formation energy being by 0.08 eV higher than that of the lowest-energy model. The other configurations are much more energetically unfavorable. For example, changing the layer sequence by placing the Sn layer on top of the Tl layer increases the formation energy by ~ 1.0 eV. Note that formation energy is defined as $E_f = E[(\text{Tl, Sn})/\text{Si}(111)] - E(\text{bulk Tl}) - E(\text{bulk Sn}) - E[\text{Si}(111)]$ and refers to the $\sqrt{3} \times \sqrt{3}$ unit cell.

For the sake of completeness, we have also applied AIRSS analysis to characterize the Tl-Sn compounds having "nonstoichiometric" compositions. The results of these evaluations are summarized in Table I which shows formation energies and lowest-energy atomic configurations obtained for the Tl-Sn compounds with various compositions. Two main conclusions can be derived based on these data. First, all the nonstoichio-

metric compounds have formation energies higher than that of the Tl(1 ML)-Sn(1 ML) compound described by the model shown in Fig. 3. Hence, one can conclude that this is the most stable (Tl, Sn)/Si(111) configuration. Second, only the Tl(1 ML)-Sn(1 ML) compound displays a sandwichlike structure. In all the other compounds the bottom layer shows up as a mixed layer where Tl and Sn atoms are intermixed. This seems reasonable as the initial Tl/Si(111)1 × 1 surface Tl atoms are bonded to Si(111) substrate while with Sn deposition Sn atoms substitute Tl in the metal-Si bonds. However, STM observations do not provide clear evidence for the formation of the well-defined intermediate phases on the way to the final Tl(1 ML)-Sn(1 ML) compound, at least at the extended regions.

With the knowledge on the atomic structure of the completed Tl-Sn compound [Fig. 3(a)], we performed the DFT calculations of its electronic properties which results are summarized in Figs. 4 and 5. In particular, Fig. 4 shows the calculated in-depth distribution of electron density. One can see that the maximal electron density is located in between Sn and Tl layers reflecting that the metallic properties of the sample is associated exactly with the 2D Tl-Sn compound. The calculated band structure is shown in Fig. 5(a), while in Fig. 5(b) the calculated dispersion curves for surface bands are superposed with the ARPES spectrum. An evident agreement between calculation results and ARPES data can serve a solid indication that the model adequately describes the (Tl, Sn)/Si(111) structure. In contrast, the calculated band structures for any other model did not fit properly the ARPES data. The calculated Fermi contours of the S_1 (S_1') surface bands shown in Fig. 5(c) demonstrates the clockwise and counterclockwise spin helicity for the inner and outer contours, respectively, while the spin out-of-plane component

is maximal at the $\overline{\Gamma}$-$\overline{M}$ directions and changes its sign while crossing zero at the $\overline{\Gamma}$-$\overline{K}$ directions [Fig. 5(d)]. Such features are known to be typically characteristic of the Rashba-split surface states at the hexagonal surfaces [18].

IV. CONCLUSIONS

In conclusion, we have demonstrated that 1 ML Tl and 1 ML Sn form a well-ordered 2D compound on Si(111) surface with a $\sqrt{3} \times \sqrt{3}$ periodicity. The 2D Tl-Sn compound is produced by depositing 1 ML Sn onto the Tl/Si(111) surface. It has a sandwichlike Tl/Sn/Si(111) structure in which Sn atoms within the bottom layer occupy basic T_1 sites and form milk-stool structure with trimers centered in H_3 sites, while Tl atoms in the top layer sit above T_4 Si(111) sites and are arranged into the honeycomb-chained-trimer structure with trimers centered also in the H_3 sites. Electronic band structure of the completed Tl-Sn compound contains two spin-split surface-state bands, of which one is nonmetallic and other is metallic. Near the Fermi level the metallic band is characterized by the the momentum splitting $\Delta k_\parallel = 0.037$ Å^{-1}, energy splitting $\Delta E_\mathrm{F} = 167$ meV, and an electron velocity of $\approx 8.5 \times 10^5$ m/s. These properties and peculiar atomic structure make the 2D Tl-Sn compound an interesting object for exploration of Rashba effect in the sandwichlike nanostructures.

[1] H. W. Yeom, S. Takeda, E. Rotenberg, I. Matsuda, K. Horikoshi, J. Schaefer, C. M. Lee, S. D. Kevan, T. Ohta, T. Nagao, and S. Hasegawa, Phys. Rev. Lett. **82**, 4898 (1999).

[2] P. C. Snijders and H. H. Weitering, Rev. Mod. Phys. **82**, 307 (2010).

[3] S. Wall, B. Krenzer, S. Wippermann, S. Sanna, F. Klasing, A. Hanisch-Blicharski, M. Kammler, W. G. Schmidt, and M. Horn-vonHoegen, Phys. Rev. Lett. **109**, 186101 (2012).

[4] H. J. Kim and J. H. Cho, Phys. Rev. Lett. **110**, 116801 (2013).

[5] I. Brihuega, O. Custance, R. Pérez, and J. M. Gómez-Rodríguez, Phys. Rev. Lett. **94**, 046101 (2005).

[6] I. Brihuega, A. Cano, M. M. Ugeda, J. J. Sáenz, A. P. Levanyuk, and J. M. Gómez-Rodríguez, Phys. Rev. Lett. **98**, 156102 (2007).

[7] M. Yakes, M. Hupalo, M. A. Zaluska-Kotur, Z. W. Gortel, and M. C. Tringides, Phys. Rev. Lett. **98**, 135504 (2007).

[8] K. L. Man, M. C. Tringides, M. M. T. Loy, and M. S. Altman, Phys. Rev. Lett. **101**, 226102 (2008).

[9] L. Huang, C. Z. Wang, M. Z. Li, and K. M. Ho, Phys. Rev. Lett. **108**, 026101 (2012).

[10] K. L. Man, M. C. Tringides, M. M. T. Loy, and M. S. Altman, Phys. Rev. Lett. **110**, 036104 (2013).

[11] K. S. Kim, S. C. Jung, M. H. Kang, and H. W. Yeom, Phys. Rev. Lett. **104**, 246803 (2010).

[12] T. Zhang, P. Cheng, W. J. Li, Y. J. Sun, G. Wang, X. G. Zhu, K. He, L. Wang, X. Ma, X. Chen, Y. Wang, Y. Liu, J. F. Jia, and Q. K. Xue, Nat. Phys. **6**, 104 (2010).

[13] T. Uchihashi, P. Mishra, M. Aono, and T. Nakayama, Phys. Rev. Lett. **107**, 207001 (2011).

[14] M. Yamada, T. Hirahara, and S. Hasegawa, Phys. Rev. Lett. **110**, 237001 (2013).

[15] S. Yoshizawa, H. Kim, T. Kawakami, Y. Nagai, T. Nakayama, X. Hu, Y. Hasegawa, and T. Uchihashi, Phys. Rev. Lett. **113**, 247004 (2014).

[16] I. Gierz, T. Suzuki, E. Frantzeskakis, S. Pons, S. Ostanin, A. Ernst, J. Henk, M. Grioni, K. Kern, and C. R. Ast, Phys. Rev. Lett. **103**, 046803 (2009).

[17] K. Sakamoto, H. Kakuta, K. Sugawara, K. Miyamoto, A. Kimura, T. Kuzumaki, N. Ueno, E. Annese, J. Fujii, A. Kodama, T. Shishidou, H. Namatame, M. Taniguchi, T. Sato, T. Takahashi, and T. Oguchi, Phys. Rev. Lett. **103**, 156801 (2009).

[18] K. Sakamoto, T. Oda, A. Kimura, K. Miyamoto, M. Tsujikawa, A. Imai, N. Ueno, H. Namatame, M. Taniguchi, P. E. J. Eriksson, and R. I. G. Uhrberg, Phys. Rev. Lett. **102**, 096805 (2009).

[19] S. D. Stolwijk, A. B. Schmidt, M. Donath, K. Sakamoto, and P. Krüger, Phys. Rev. Lett. **111**, 176402 (2013).

[20] J. Park, S. W. Jung, M. C. Jung, H. Yamane, N. Kosugi, and H. W. Yeom, Phys. Rev. Lett. **110**, 036801 (2013).

[21] K. Yaji, Y. Ohtsubo, S. Hatta, H. Okuyama, K. Miyamoto, T. Okuda, A. Kimura, H. Namatame, M. Taniguchi, and T. Aruga, Nat. Commun. **1**, 17 (2010).

[22] P. Höpfner, J. Schäfer, A. Fleszar, J. H. Dil, B. Slomski, F. Meier, C. Loho, C. Blumenstein, L. Patthey, W. Hanke, and R. Claessen, Phys. Rev. Lett. **108**, 186801 (2012).

[23] L. V. Bondarenko, D. V. Gruznev, A. A. Yakovlev, A. Y. Tupchaya, D. Usachov, O. Vilkov, A. Fedorov, D. V. Vyalikh, S. V. Eremeev, E. V. Chulkov, A. V. Zotov, and A. A. Saranin, Sci. Rep. **3**, 1826 (2013).

[24] J. R. Osiecki, H. M. Sohail, P. E. J. Eriksson, and R. I. G. Uhrberg, Phys. Rev. Lett. **109**, 057601 (2012).

[25] M. Zhou, W. Ming, Z. Liu, Z. Wang, P. Li, and F. Liu, PNAS **111**, 14378 (2014).

[26] M. Zhou, W. Ming, Z. Liu, Z. Wang, Y. Yao, and F. Liu, Sci. Rep. **4**, 7102 (2014).

[27] D. V. Gruznev, L. V. Bondarenko, A. V. Matetskiy, A. A. Yakovlev, A. Y. Tupchaya, S. V. Eremeev, E. V. Chulkov, J. P.

Chou, C. M. Wei, M. Y. Lai, Y. L. Wang, A. V. Zotov, and A. A. Saranin, Sci. Rep. **4**, 4742 (2014).

[28] P. E. Blöchl, Phys. Rev. B **50**, 17953 (1994).

[29] G. Kresse and D. Joubert, Phys. Rev. B **59**, 1758 (1999).

[30] G. Kresse and J. Hafner, Phys. Rev. B **49**, 14251 (1994).

[31] G. Kresse and J. Furthmüller, Comp. Mater. Sci. **6**, 15 (1996).

[32] C. J. Pickard and R. J. Needs, J. Phys.: Condens. Matter **23**, 053201 (2011).

[33] C. J. Pickard and R. J. Needs, Phys. Rev. Lett. **97**, 045504 (2006).

[34] A. J. Morris, C. J. Pickard, and R. J. Needs, Phys. Rev. B **78**, 184102 (2008).

[35] D. V. Gruznev, A. V. Matetskiy, L. V. Bondarenko, O. A. Utas, A. V. Zotov, A. A. Saranin, J. P. Chou, C. M. Wei, M. Y. Lai, and Y. L. Wang, Nat. Commun. **4**, 1679 (2013).

[36] J. P. Chou, C. M. Wei, Y. L. Wang, D. V. Gruznev, L. V. Bondarenko, A. V. Matetskiy, A. Y. Tupchaya, A. V. Zotov, and A. A. Saranin, Phys. Rev. B **89**, 155310 (2014).

[37] J. P. Chou, C. R. Hsing, C. M. Wei, C. Cheng, and C. M. Chang, J. Phys.: Condens. Matter **25**, 125305 (2013).